Int. J. Nonlinear Anal. Appl. 14 (2023) 3, 353–367
ISSN: 2008-6822 (electronic)
http://dx.doi.org/10.22075/ijnaa.2022.24856.2841

Solving partial-differential algebraic equations with the fifth-Order Meshless Petrov-Galerkin Method by CS-RBFS interpolation

Azam Noorafkan Zanjani[a], Saeid Abbasbandy[b,*], Fahimeh Soltanian[a]

[a]*Department of Mathematics, Payame Noor University (PNU), P.O.Box 19395-4697, Tehran, Iran*

[b]*Department of Applied Mathematics, Faculty of Science, Imam Khomeini International University, Qazvin 34149-16818, Iran*

(Communicated by Haydar Akca)

Abstract

In this paper, the application of the Fifth-order Meshless Local Petrov-Galerkin Method in solving the linear partial differential-algebraic equations (PDAEs) was surveyed. The Gaussian quadrature points in the domain and on the boundary were determined as centers of local sub-domains. By governing the local weak form in each sub-domain, the compactly supported radial basis functions (CS-RBFs) approximation was used as the trial function and the Heaviside step function was considered as the test function. The proposed method was successfully utilized for solving linear PDAEs and the numerical results were obtained and compared with the exact solution to investigate the accuracy of the proposed method. The sensitivity to different parameters was analyzed and a comparison with the other methods was done.

Keywords: Partial Differential Algebraic Equations, Meshless Local Petrov-Galerkin Method, Radial Basis Functions
2020 MSC: 65L80, 65M99

1 Introduction

In the past decades, meshless methods in solving the boundary value problems have received much attention due to their flexibility and overcoming difficulties depend on meshing or re-meshing because there is no need to generate any mesh and it only uses arbitrarily scattering points in the domain, so the meshless methods have the advantage in solving problems numerically with the complex domain. However, in those meshless methods which have been developed before 1998, the meshless technique had been used only for interpolating the trial function and it still needed to use the background meshes for integration of the weak-form. Therefore, those methods are not considered truly meshless. Since 1998, Atluri and his colleagues [4, 8, 7, 5, 9, 6] have developed two truly meshless method for solving linear and nonlinear boundary problems: the meshless local Petrov-Galerkin (MLPG) method and the meshless local boundary integral equation (LBIE) method. The main objective of MLPG methods is no domain or

*Corresponding author
Email addresses: azam57@gmail.com (Azam Noorafkan Zanjani), abbasbandy@sci.ikiu.ac.ir (Saeid Abbasbandy), f_soltanian@pnu.ac.ir (Fahimeh Soltanian)

Received: October 2021 *Accepted:* January 2022

boundary meshes are required even for integration of the weak-form, and all relevant integrals can be easily evaluated over domains and their boundaries. There are many applications of this method [2, 14].

The radial basis functions (RBFs) have been employed for solving partial differential equations using MLPG methods in [3, 4, 17, 26]. Also, it became popular as an excellent interpolation property and has great promise in MLPG and other meshless methods due to their effectiveness in interpolating multivariate scattered data. However, the RBF interpolation may suffer from the contradiction between the accuracy and the stability, which can be described as uncertainly principle [20]. The condition number of the RBF interpolation matrix becomes very large when the interpolation points are irregularly or density arranged, and the ill-conditioned matrix will limit the application of the RBF, especially for large-scale problems. In order to guarantee the robustness and the stability of interpolation with RBFs, many numerical treatments have been proposed such as: compactly supported RBF method [15], precondition method [16], domain decomposition method [12], RBF with variable shape parameter method [27] and node adoptively method [13].

Many important mathematical, engineering, physical science, and population growth models can be expressed in terms of time-dependent systems of differential-algebraic equations (DAEs). DAEs include ordinary differential equations (ODEs) with finite-dimensional algebraic equations. Partial differential equations (PDEs) which lead to DAEs are often called PDAEs. Many detailed index analyses of the DAEs and PDAEs with respect to the modal index, algebraic index, and the index by means of the method of lines approach for PDAEs and some numerical methods were investigated in [21, 11].

In this paper, we apply the MLPG5 from Atluri [4, 6] which uses local weighted residual form (LWF) and the Heaviside step function as the test function over a local sub-domain and a local interpolation based on the compactly supported radial basis functions, for solving the time-dependent linear PDAEs.

2 Partial differential algebraic equations

Consider the following linear PDAE in the domain Ω bounded by the boundary Γ [18]:

$$A\Psi_t(x,t) + B\Psi_{xx}(x,t) + C\Psi_x(x,t) + D\Psi(x,t) = P(x,t), \tag{2.1}$$

where

$$t \in [t_0, t_f] \quad , \quad x \in [x_1, x_2] \quad , \quad A, B, C, D \in \mathbb{R}^{n\times n},$$

and

$$\Psi, P : [x_1, x_2] \times [t_0, t_f] \to \mathbb{R}^n.$$

If $A = 0$ or $B = 0$ & $C = 0$, then we have ODEs or DAEs. In general, the above differential equation is required to satisfy the following boundary and initial conditions

$$E\Psi(x,t) + F\frac{\partial \Psi(x,t)}{\partial n} = \mathbf{q}(x,t), \tag{2.2}$$

where $t \in [t_0, t_f]$, $x \in \Gamma$ and

$$\Psi(x, t_0) = \Psi_0(x), \tag{2.3}$$

where E and F are known constant matrices and $\mathbf{q} : [x_1, x_2] \times [t_0, t_f] \to \mathbb{R}^n$ and Ψ_0 are known functions and $\frac{\partial \Psi(x,t)}{\partial n}$ is the outward normal derivative.

When $F = 0$ and $E \neq 0$ it is called Dirichlet type of boundary condition, when $F \neq 0$ and $E = 0$ it is called Neumann type and when $F \neq 0$ and $E \neq 0$ it is called mixed or Robin type. Marszalek [18] has proposed the definition of the modal index for PDAEs (2.1) with $C = 0$, $x_1 = 0$ and $x_2 = l$. The boundary and initial conditions are

$$\Psi(0,t) = 0,\ \Psi(l,t) = 0 \text{ and } \Psi(x,0) = \mathbf{q},$$

where P and $\mathbf{q}$ are smooth enough and are consistent with the boundary and initial conditions.

3 Compactly Supported Radial Basis Functions

3.1 CS-RBFs interpolation

Interpolation by radial functions has been used as a powerful tool in multivariate approximation theory, especially since CS-RBFs have been derived. The CS-RBFs were demonstrated that for a given dimension and smoothness C^{2p},

a positive definite radial basis function in the form of a univariate polynomial of minimal degree always exists, and is unique within a constant factor [8]. According to the different type of radial basis functions of compact support which were proposed by Wendland ($\zeta^1 - \zeta^4$) [22] and Wu (ζ^5, ζ^6) [25], we apply CS-RBFs that provided by Wu as follow:

$$
\begin{aligned}
\zeta_i^1(\mathbf{x}) &= (1-\frac{\delta_i}{s_i})^2, && 0 \le \delta_i \le s_i,\\
\zeta_i^2(\mathbf{x}) &= (1-\frac{\delta_i}{s_i})^4(1+4\frac{\delta_i}{s_i}), && 0 \le \delta_i \le s_i,\\
\zeta_i^3(\mathbf{x}) &= (1-\frac{\delta_i}{s_i})^6(3+18\frac{\delta_i}{s_i}+35\frac{\delta_i^2}{s_i^2}), && 0 \le \delta_i \le s_i,\\
\zeta_i^4(\mathbf{x}) &= (1-\frac{\delta_i}{s_i})^8(1+8\frac{\delta_i}{s_i}+25\frac{\delta_i^2}{s_i^2}++32\frac{\delta_i^3}{s_i^3}), && 0 \le \delta_i \le s_i,\\
\zeta_i^5(\mathbf{x}) &= (1-\frac{\delta_i}{s_i})^5(8+40\frac{\delta_i}{s_i}+48\frac{\delta_i^2}{s_i^2}+25\frac{\delta_i^3}{s_i^3}+5\frac{\delta_i^4}{s_i^4}), && 0 \le \delta_i \le s_i,\\
\zeta_i^6(\mathbf{x}) &= (1-\frac{\delta_i}{s_i})^6(6+36\frac{\delta_i}{s_i}+82\frac{\delta_i^2}{s_i^2}+72\frac{\delta_i^3}{s_i^3}+30\frac{\delta_i^4}{s_i^4}+5\frac{\delta_i^5}{s_i^5}), && 0 \le \delta_i \le s_i,
\end{aligned}
\tag{3.1}
$$

otherwise

$$\zeta_i^k(\mathbf{x}) = 0 \quad \text{for} \quad k = 1, \ldots, 6,$$

where

- δ_i is the distance from $\mathbf{x}$ to $\mathbf{x}_i$,
- s_i is the size of support for RBF at node $\mathbf{x}_i$,
- $\mathbf{x}_i$ is the i-th node.

If Φ_i is the approximation function in the sub-domain $\Omega_s^{(i)}$, then the radial basis approximation can be written as

$$\Phi_i(\mathbf{x}) = \zeta(\mathbf{x})\mathbf{a}, \qquad \mathbf{x} \in \Omega_s^{(i)},$$

over a number of scattered nodes $\mathbf{x}_i$ for $i = 1, \ldots, Q$.
After interpolating for CS-RBF, we will have a system of linear equations

$$\zeta_0 \mathbf{a} = \Phi, \tag{3.2}$$

where

$$\Phi = \begin{pmatrix} \phi_1 \\ \phi_2 \\ \cdots \\ \phi_Q \end{pmatrix}, \quad \zeta_0 = \begin{pmatrix} \zeta_1(\mathbf{x}_1) & \zeta_2(\mathbf{x}_1) & \cdots & \zeta_Q(\mathbf{x}_1) \\ \zeta_1(\mathbf{x}_2) & \zeta_2(\mathbf{x}_2) & \cdots & \zeta_Q(\mathbf{x}_2) \\ \vdots & \vdots & \vdots & \vdots \\ \zeta_1(\mathbf{x}_Q) & \zeta_2(\mathbf{x}_Q) & \cdots & \zeta_Q(\mathbf{x}_Q) \end{pmatrix},$$

and $\zeta^T(\mathbf{x}) = [\zeta_1(\mathbf{x}), \zeta_2(\mathbf{x}), \cdots, \zeta_N(\mathbf{x})]$ is the set of RBFs centered around $\mathbf{x}_i$, $\mathbf{a}$ is the coefficient vector and Φ_i for $i = 1, \cdots, Q$, are the nodal values.
Since the RBFs are positive definite, the matrix ζ_0 is non-singular. So, by multiplying the ζ_0^{-1} to equation (3.2), we obtain

$$\mathbf{a} = \zeta_0^{-1}\Phi. \tag{3.3}$$

Thus, the approximation $\Phi(\mathbf{x})$ can be written as

$$\Phi(\mathbf{x}) = \zeta\ \zeta_0^{-1}\Phi = \sum_{i=1}^{Q} \chi_i(\mathbf{x})\Phi, \tag{3.4}$$

where $\chi(\mathbf{x}) = \zeta(\mathbf{x})\zeta_0^{-1}$ is the nodal shape function which depends uniquely on the distribution of scattered nodes in sub-domains and possess the Kronecker Delta property. The nodal shape functions can be written as

$$\chi_i(\mathbf{x}) = \sum_{j=1}^{Q} \zeta_j(\mathbf{x})(\zeta_0^{-1})_{ji}.$$

In addition, the partial derivative of the shape function is

$$\frac{\partial \chi(\mathbf{x})}{\partial x_k} = \frac{\partial \zeta(\mathbf{x})}{\partial x_k}\zeta_0^{-1} = \left[\frac{\partial \zeta_1(\mathbf{x})}{\partial x_k} \quad \frac{\partial \zeta_2(\mathbf{x})}{\partial x_k} \quad \cdots \quad \frac{\partial \zeta_Q(\mathbf{x})}{\partial x_k}\right]\zeta_0^{-1}, \quad k = 1, \ldots, n,$$

where

$$\frac{\partial \chi_j(\mathbf{x})}{\partial x_k} = \sum_{i=1}^{Q} \frac{\partial \zeta_i(\mathbf{x})}{\partial x_k}(\zeta_0^{-1})_{ij}, \quad j = 1, \ldots, Q, \tag{3.5}$$

and

$$\frac{\partial \zeta_i(\mathbf{x})}{\partial x_k} = \frac{\partial \zeta_i(\mathbf{x})}{\partial \delta_i}\frac{\partial \delta_i}{\partial x_k} \quad \text{with} \quad \frac{\partial \delta_i}{\partial x_k} = \frac{x_k - x_k^i}{\delta_i}.$$

3.2 Stability analysis

Definition 3.1. Let the operator I and its inverse D be defined as follow:

$$I\{\xi(\delta)\} = \int_{\delta}^{\infty} y\xi(y)dy,$$
$$D\{\xi(\delta)\} = -\frac{1}{\delta}\xi^{'}(y).$$

We introduce $\xi_{n,p} = I^p \xi_{\left[\frac{n}{2}\right]+p+1}$ where, $\xi_p = (1-\delta)_+^p$ and

$$\xi_{n,p}(\delta) = \begin{cases} \zeta^j(\delta), & 0 \le \delta \le 1, \\ 0, & 1 \le \delta, \end{cases}$$

which $\zeta^j(\delta)$ for $j = 1, \ldots, 6$ in the (3.1) are univariate polynomials of degree $\left[\frac{n}{2}\right] + p + 1$ and smoothness $2p$.

Definition 3.2. For an integrable and positive definite function $g : \mathbb{R}^n \to \mathbb{R}$ with non-negative and non-vanishing Fourier transform

$$\tilde{g}(\nu) = (\frac{1}{2\pi})^{\frac{n}{2}} \int_{\mathbb{R}^n} g(\mathbf{x}) e^{-i\mathbf{x}^T\nu}\, d\mathbf{x},$$

we define the univariate operator $F_n\{\xi(\delta)\}$ as follow:

$$F_n\{\xi(\delta)\} \equiv \tilde{g}(\nu) = (\frac{1}{2\pi})^{\frac{n}{2}} \int_{\mathbb{R}^n} g(\mathbf{x}) e^{-i\mathbf{x}^T\nu}\, d\mathbf{x} = (\frac{1}{\delta})^{\frac{n}{2}-1} \int_0^{\infty} \xi(y) y^{\frac{n}{2}} J_{\frac{n}{2}-1}(\delta y)\, dy,$$

where $\xi(\delta) = g(\mathbf{x})$, $\delta = ||\mathbf{x} - \mathbf{x}_i||_2$ and

$$J_\alpha(\nu) = \sum_{i=0}^{\infty} \frac{(-1)^i (\frac{\nu}{2})^{\alpha+2i}}{i!\Gamma(\alpha + i + 1)},$$

is the Bessel function of the first type. Also, we have

$$F_n\{I\{\xi(\delta)\}\} = F_{n+2}\{\xi(\delta)\}, \quad \text{and} \quad F_n\{D\{\xi(\delta)\}\} = F_{n+2}\{\xi(\delta)\}.$$

Definition 3.3. For a set of centers $S = \{\mathbf{x}_1, \mathbf{x}_2, ..., \mathbf{x}_m\} \subseteq \Omega \subseteq \mathbb{R}^n$, the density measure is defined in the form of

$$h_0 = \sup_{\mathbf{x}\in\Omega} \min_{1\le i\le m} ||\mathbf{x} - \mathbf{x}_i||_2.$$

Lemma 3.4. For $r \in \mathbb{N}$, there exists a δ_r that

$$\frac{1}{\pi\delta} \le J_{r+\frac{1}{2}}^2(\delta) + J_{r+\frac{3}{2}}^2(\delta),$$

for all $\delta \ge \delta_r$.

Theorem 3.5. Suppose the Hilbert space R_g include all $\Psi : \mathbb{R}^n \to \mathbb{R}$, with Fourier transform $\tilde{\Psi}$, which

$$\Psi(\mathbf{x}) = (\frac{1}{2\pi})^{\frac{n}{2}} \int_{\mathbb{R}^n} \tilde{\Psi}(\nu) e^{i\mathbf{x}^T\nu}\, d\nu,$$

and

$$\tilde{\Psi}/\sqrt{\tilde{g}} \in L_2(\mathbb{R}^n),$$

with the norm

$$||\Psi||_g = (\frac{1}{2\pi})^{\frac{n}{4}} \left(\int_{\mathbb{R}^n} \frac{|\tilde{\Psi}(\nu)|^2}{\tilde{g}(\nu)}\, d\nu \right)^{\frac{1}{2}}.$$

For every $h \le h_0$ and $\Psi \in R_g$, whose corresponding CS-RBFs approximation is Φ, the estimate error

$$||\Psi - \Phi||_\infty \le C||\Psi||_g h^k,$$

holds.

Proof . Let $l = [\frac{n}{2}] + p + 1$. Then we have

$$F_n\{\xi_{n,p}(\delta)\} = F_n\{I^p\{\xi_l(\delta)\}\} = F_{n+2p}\{\xi_l(\delta)\} = (\frac{1}{\delta})^{-n-2p-1} \int_0^\delta (\delta - t)^l t^{\frac{n}{2}+p} J_{\frac{n}{2}+p-1}(t)\, dt.$$

If $n = 2k + 1$ and $r = p + k$, then $l = r + 1$. Therefore,

$$F_n\{\xi_{n,p}(\delta)\} = F_{2k+1}\xi_{n,p}(\delta) = (\frac{1}{\delta})^{3r+2} \int_0^\delta (\delta - t)^{r+1} t^{r+\frac{1}{2}} J_{r-\frac{1}{2}}(t)\, dt. \tag{3.6}$$

After integration by parts, we obtain

$$\begin{aligned} F_n\{\xi_{n,p}(\delta)\} &= (\frac{1}{\delta})^{3r+2} \left(-(r+1)(\delta - t)^r t^{r+\frac{1}{2}} J_{r+\frac{1}{2}}(t)|_0^\delta + (r+1) \int_0^\delta (\delta - t)^r t^{r+\frac{1}{2}} J_{r+\frac{1}{2}}(t)\, dt \right) \\ &= (\frac{1}{\delta})^{3r+2} (r+1) \int_0^\delta (\delta - t)^r t^{r+\frac{1}{2}} J_{r+\frac{1}{2}}(t)\, dt. \end{aligned}$$

According to Lemma 3.1 in [23], we get

$$\begin{aligned} F_n\{\xi_{n,p}(\delta)\} &= (\frac{1}{\delta})^{3r+2}(r+1) \frac{\Gamma(r+1)\Gamma(2r+2)\Gamma(r+\frac{3}{2})}{\Gamma(3r+3)} 2^{3r+\frac{3}{2}} \delta^{r+1} \times \sum_{j=0}^{\infty} \frac{(\frac{r+1}{2})_j (\frac{r}{2})_j}{(\frac{3r+3}{2})_j} \frac{(2r+2)_j}{j!} \frac{2j+2r+1}{j+2r+1} J^2_{r+j+\frac{1}{2}}(\frac{\delta}{2}) \\ &\ge C\delta^{-2r-1} \times \left(J^2_{r+\frac{1}{2}}(\frac{\delta}{2}) + J^2_{r+\frac{3}{2}}(\frac{\delta}{2}) \right) \\ &\ge C\delta^{-2r-1} \times \left(\frac{1}{\pi\delta} \right), \end{aligned}$$

which implies

$$F_n\{\xi_{n,p}(\delta)\} \ge C_1 \delta^{-n-2p-1}. \tag{3.7}$$

The proof of lower bound for $F_n\{\xi_{n,p}\}$ is complete. In order to find the upper bound, we introduce the function q_r as

$$q_r = \begin{cases} 1 - cos(\delta), & r = 0, \\ q_0 * q_{r-1}(\delta), & r \ge 0. \end{cases} \tag{3.8}$$

By calculating the Laplace transform, we get

$$L\{q_r\} = L\{q_0 * q_{r-1}(\delta)\} = L\{\int_0^\delta q_0(t) q_{r-1}(\delta - t)\, dt\} = \frac{1}{s^{r+1}(1+s^2)^{r+1}}.$$

On the other hand,

$$\begin{aligned} L\{\int_0^\delta (\delta-t)^{r+1}t^{r+\frac{1}{2}}J_{r-\frac{1}{2}}(t)\ dt\} &= \frac{r!(r+1)!2^{r+\frac{1}{2}}}{\sqrt{\pi}s^{r+1}(1+s^2)^{r+1}} \\ &= A_r\frac{1}{s^{r+1}(1+s^2)^{r+1}} \\ &= A_rL\{q_r(\delta)\} \\ &= L\{A_rq_r(\delta)\}. \end{aligned}$$

Thus, we conclude that

$$\int_0^\delta (\delta-t)^{r+1}t^{r+\frac{1}{2}}J_{r-\frac{1}{2}}(t)\ dt = A_rq_r(\delta). \tag{3.9}$$

By substituting (3.9) in (3.6), we have

$$\begin{aligned} F_n\{\xi_{n,p}\}(\delta) &= (\frac{1}{\delta})^{3r+2}\int_0^\delta (\delta-t)^l t^{r+\frac{1}{2}}J_{r-\frac{1}{2}}(t)\,dt \\ &= (\frac{1}{\delta})^{3r+2}A_rq_r(\delta) \\ &\leq C_2\delta^{-n-2p-1}. \end{aligned}$$

Now, set $n=2k$. And $r=p+k$. Also, we consider

$$F_n\{\xi_{n,p}\}(\delta) = (\frac{1}{\delta})^{3r+1}\int_0^\delta (\delta-t)^{r+1}t^rJ_{r-1}(t)\,dt,$$

and

$$q_r(\delta) = \begin{cases} \int_0^\delta J_0(t),\ dt & r=0, \\ q_0 * q_{r-1}(\delta), & r\geq 0. \end{cases}$$

Analogously, we can obtain $F_n\{\xi_{n,p}\}(\delta) = (\frac{1}{\delta})^{3r+2}A_rq_r(\delta)$ for $n=2k$. Consequently, for every space dimension n and arbitrary $p\in\mathbb{N}_0$, there are constants δ_0, C_1 and C_2 depending only on dimension n and p such that for the Fourier transform of $\xi_{n,p}$:

$$F_n\{\xi_{n,p}\}(\delta) \geq C_1\delta^{-n-2p-1}, \tag{3.10}$$

and for every $\delta\geq\delta_0$, we have

$$F_n\{\xi_{n,p}\}(\delta) \leq C_2\delta^{-n-2p-1}. \tag{3.11}$$

Inequities (3.10) and (3.11) show that the Fourier transform $\tilde{g}$ has the asymptotic behaviour

$$\tilde{g}(\nu) = O(||\nu||_2^{-n-\alpha}) \quad \text{as} \quad ||\nu||_2\to\infty. \tag{3.12}$$

Thus, from [24] and (3.12), we get

$$||\Psi-\Phi||_\infty \leq C_0||\Psi||_g h^{\frac{\alpha}{2}},$$

for every $h\leq h_0$ and $\Psi\in R_g$. □

4 Implementing MLPG to PDAEs

4.1 MLPG

Contrary to the Galerkin finite element and element free Galerkin which we consider the global weak-form over the entire domain Ω for numerically solving the problem, in MLPG method formulation, we work on the weak-form of the problem over a certain number of sub-domain Ω_s and implement the compactly supported radial basis functions approximation for trial function.

Given that the shape and the size of sub-domains have no effect on the answer, in MLPG methods typically the sub-domains are considered a circle in 2D and a sphere in 3D with the center at the $N\times M=Q$ nodes $\mathbf{x_i}$,

$i = 1, \cdots, Q$, and fix radius r_0 in entire domain and boundary. The most significant difference between this method and the finite element method or any other meshless method is that the local weak-forms are generated on overlapping local sub-domains instead of using the global weak-form [1].

Integration of the weak-form is performed in local sub-domains with simple geometrical shapes. Therefore, no elements or background cells are necessary either for interpolation purposes or for integration purposes. The local sub-domain Ω_s can have an arbitrary shape, but it is typically considered as a circle centered at each node $\mathbf{x_i}$ with a fixed radius r_0 as we have chosen in this paper.

The meshless local Petrov-Galerkin approach is based on asymmetric weak-form (4.3) which was discussed in detail in [8, 7]. Choosing the trial function and the test function from different spaces is one of the notable features of the MLPG methods. In particular, the test function should not vanish on the boundary where the essential boundary conditions are defined. In the present paper, we selected the Heaviside step function as the test function and CS-RBFs as the trial function in each sub-domain base on the method which was introduced as MLPG5 method in Atluri and Shen's results [6].

4.2 Local weak-formulation

Lemma 4.1. Suppose that Ω is an open bounded subset of $\mathbb{R}^n$ with piecewise smooth boundary $\Gamma = \partial\Omega$ or the boundary only is Lipschitz continuous and the scalar-valued function u and vector-valued function V lie in the Sobolev space. Then,

$$\int_\Omega u\ \nabla \cdot V\, d\Omega = \int_\Gamma u\ V \cdot \hat{n}\, d\Gamma - \int_\Omega \nabla u \cdot V\, d\Omega.$$

Proof . For the scalar-valued function u and vector-valued function V, the product divergence rule is

$$\nabla(uV) = u\nabla V + \nabla u \cdot V.$$

If Ω is an open bounded subset of $\mathbb{R}^n$ with boundary Γ, then after integrating over Ω with respect to the standard volume form of Ω and applying divergence theorem, we obtain

$$\int_\Gamma u\ V \cdot \hat{n}\, d\Gamma\ = \int_\Omega \nabla(uV)\, d\Omega\ = \int_\Omega u\nabla \cdot V\, d\Omega\ + \int_\Omega \nabla u \cdot V\, d\Omega, \tag{4.1}$$

then by rearranging the equation (4.1), the proof is complete. $\hat{n}$ is the outward unit normal vector to the boundary. □

Theorem 4.2. The local weak-form formula for problem (2.1) with boundary conditions (2.2) and initial conditions (2.3) in each sub-domain Ω_s is as follow:

$$\int_{\Gamma_{su}} q\, d\Gamma + \int_{L_s} q\, d\Gamma + D\int_{\Omega_s} \varphi\, d\Omega - \eta\int_{\Gamma_{su}} \varphi\, d\Gamma = \eta\int_{\Gamma_{su}} \varphi_0 + \int_{\Gamma_{sq}} \bar{q}\, d\Gamma - \int_{\Omega_s} P\, d\Omega. \tag{4.2}$$

Proof . Let φ be the trial function and approximate solution to present considered PDAEs (2.1). In each sub-domain $\Omega_s^{(i)}$ with $i = 1, \ldots, M$, we write the local weak-forms as

$$\int_{\Omega_s} [A\varphi_t(x,t) + B\varphi_{xx}(x,t) + C\varphi_x(x,t) + D\varphi(x,t) - P(x,t)]\mu\, d\Omega - \eta\int_{\Gamma_{su}} [\varphi(x,t) - \varphi(x,t_0)]\mu\, d\Gamma = 0,$$

where

- μ is the test function,
- L_s is a part of local boundary over which no boundary condition is specified,
- Γ_{sq} is a part of local boundary over which natural boundary condition is specified,
- Γ_u is the global boundary over which essential boundary condition is specified,
- Γ_{su} is the part of the local boundary over which essential boundary condition is specified,

- $\eta >> 1$ is a penalty parameter which is used to impose the essential boundary conditions.

The boundary Ω_s generally consists of a part L_s located inside the global domain, where no boundary conditions are specified. Γ_{su} and Γ_{sq} located on the global domain boundary Γ, where Dirichlet and Neumann boundary conditions are given, respectively. For Ω_s located entirely within Ω, there is no intersection between Ω_s and Γ, hence the integrals over Γ_{su} and Γ_{sq} vanish. Also the boundary integrals over Γ_{su} and Γ_{sq} vanish for those sub-domains which entirely are located in the global domain and there are not any intersection between them and the global domain.

By using the Lemma 4.1 for the local weak-form formula, we obtain the following equation:

$$A\int_{\Gamma_s}\varphi\mu\cdot n_j\,d\Gamma - A\int_{\Omega_s}\varphi\mu_t\,d\Omega + B\int_{\Gamma_s}\varphi_x\mu\cdot n_i\,d\Gamma - B\int_{\Omega_s}\varphi_x\mu_x\,d\Omega + C\int_{\Gamma_s}\varphi\mu\cdot n_i\,d\Gamma$$
$$-C\int_{\Omega_s}\varphi\mu_x\,d\Omega + D\int_{\Omega_s}\varphi\mu\,d\Omega - \int_{\Omega_s}P\mu\,d\Omega - \eta\int_{\Gamma_{su}}\varphi\mu\,d\Gamma + \eta\int_{\Gamma_{su}}\varphi_0\mu\,d\Gamma = 0.$$

Thus,

$$\int_{\Gamma_s}(A\varphi\delta_{ij} + B\varphi_x + C\varphi)\mu.n_i\,d\Gamma - A\int_{\Omega_s}\varphi\mu_t\,d\Omega - B\int_{\Omega_s}\varphi_x\mu_x\,d\Omega - C\int_{\Omega_s}\varphi\mu_x\,d\Omega$$
$$+D\int_{\Omega_s}\varphi\mu\,d\Omega - \int_{\Omega_s}P\mu\,d\Omega - \eta\int_{\Gamma_{su}}\varphi\mu\,d\Gamma + \eta\int_{\Gamma_{su}}\varphi_0\mu\,d\Gamma = 0. \tag{4.3}$$

The LSWF is simplified as the following equation:

$$\int_{\Gamma_s}(A\varphi\delta_{ij} + B\varphi_x + C\varphi).n_i\,d\Gamma + D\int_{\Omega_s}\varphi\,d\Omega - \int_{\Omega_s}P\,d\Omega - \eta\int_{\Gamma_{su}}\varphi\,d\Gamma + \eta\int_{\Gamma_{su}}\varphi_0\,d\Gamma = 0,$$

where

$$\mu = \begin{cases} 1, & x \in \Omega_s, \\ 0, & x \notin \Omega_s. \end{cases}$$

According to the sub-domains boundary, we have

$$\int_{\Gamma_{sq}}(A\varphi\delta_{ij} + B\varphi_x + C\varphi)\cdot n_i\,d\Gamma + \int_{\Gamma_{su}}(A\varphi\delta_{ij} + B\varphi_x + C\varphi)\cdot n_i\,d\Gamma + \int_{L_s}(A\varphi\delta_{ij} + B\varphi_x + C\varphi)\cdot n_i\,d\Gamma$$
$$+D\int_{\Omega_s}\varphi\,d\Omega - \int_{\Omega_s}P\,d\Omega - \eta\int_{\Gamma_{su}}\varphi\,d\Gamma + \eta\int_{\Gamma_{su}}\varphi_0\,d\Gamma = 0.$$

After imposing the Neumann boundary conditions $(A\varphi\delta_{ij} + B\varphi_x + C\varphi)\cdot n_i \equiv q = \bar{q}$ on Γ_{sq}, we have

$$\int_{\Gamma_{sq}}\bar{q}\,d\Gamma + \int_{\Gamma_{su}}q\,d\Gamma + \int_{L_s}q\,d\Gamma + D\int_{\Omega_s}\varphi\,d\Omega - \int_{\Omega_s}P\,d\Omega - \eta\int_{\Gamma_{su}}\varphi\,d\Gamma + \eta\int_{\Gamma_{su}}\varphi_0\,d\Gamma = 0,$$

which indicates that (4.2) is valid. □

4.3 Domain discretization

In the MLPG5 method, after substituting the CS-RBF approximations (3.4) and (3.5) to approximate the trial function in each sub-domain Ω_s into the local symmetric weak-form equation (4.2) leads to following linear system:

$$\sum_{i=1}^{Q}\int_{\Gamma_{su}}\Big(A\chi_i(\mathbf{x})\phi_i\delta_{ij} + B\frac{\partial\chi_i(\mathbf{x})}{\partial x}\phi_i + C\chi_i(\mathbf{x})\phi_i\Big)n_i\,d\Gamma + \sum_{i=1}^{Q}\int_{L_s}\Big(A\chi_i(\mathbf{x})\phi_i\delta_{ij} + B\frac{\partial\chi_i(\mathbf{x})}{\partial n}\phi_i + C\chi_i(\mathbf{x})\phi_i\Big)n_i\,d\Gamma +$$
$$D\sum_{i=1}^{Q}\int_{\Omega_s}\chi_i(\mathbf{x})\phi_i\,d\Omega - \eta\sum_{i=1}^{Q}\int_{\Gamma_{su}}\chi_i(\mathbf{x})\phi_i\,d\Omega = \eta\int_{\Gamma_{su}}\varphi_0 + \int_{\Gamma_{sq}}\bar{\mathbf{q}}\,d\Gamma - \int_{\Omega_s}P\,d\Omega. \tag{4.4}$$

In the simplified form is

$$\mathbf{K\Phi} = \mathbf{f}, \tag{4.5}$$

where $\mathbf{K}$ is the global stiffness matrix and $\mathbf{f}$ is the global load vector.

4.4 Governing equations

Considering two types of nodes in domain and boundary in the current method,

(i) The first type is the internal nodes whose local sub-domains have no intersection with the global boundary (Note: for the nodes are located close to the global boundary but not exactly on the global boundary, the radius is considered small enough not to cross the boundary),

(ii) The second type is the boundary nodes whose exactly are located on global boundary,

in linear system (4.5) the governing of the equation of the first type becomes simpler and the entries of the global stiffness matrix $\mathbf{K}$ and the global load vector $\mathbf{f}$ are defined by

$$\begin{aligned} K_{ij} &= \int_{L_s} \Big(A\chi_i(\mathbf{x}_j)\delta_{ij} + B\frac{\partial \chi_i(\mathbf{x}_j)}{\partial n} + C\chi_i(\mathbf{x}_j) \Big) n_i \, d\Gamma \; + D \int_{\Omega_s} \chi_i(\mathbf{x}_j) \, d\Omega, \\ f_i &= -\int_{\Omega_s} P \, d\Omega, \end{aligned} \tag{4.6}$$

and in the case of the second type of nodes are defined by

$$\begin{aligned} K_{ij} &= \int_{\Gamma_{su}} \Big(A\chi_i(\mathbf{x}_j)\delta_{ij} + B\frac{\partial \chi_i(\mathbf{x}_j)}{\partial x} + C\chi_i(\mathbf{x}_j) \Big) n_i \, d\Gamma + \int_{L_s} \Big(A\chi_i(\mathbf{x}_j)\delta_{ij} + B\frac{\partial \chi_i(\mathbf{x}_j)}{\partial n} + C\chi_i(\mathbf{x}_j) \Big) n_i \, d\Gamma \\ &\quad + D \int_{\Omega_s} \chi_i(\mathbf{x}_j) \, d\Omega - \eta \int_{\Gamma_{su}} \chi_i(\mathbf{x}_j) \, d\Omega, \\ f_i &= \eta \int_{\Gamma_{su}} \varphi_0 \, d\Gamma + \int_{\Gamma_{sq}} \bar{\mathbf{q}} \, d\Gamma - \int_{\Omega_s} P \, d\Omega. \end{aligned} \tag{4.7}$$

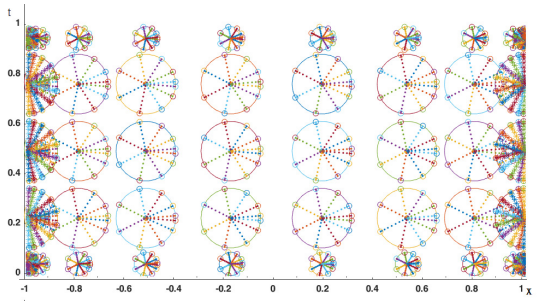

Figure 1: Distribution of Gaussian points in domain $N = 8 \times 5$ and circular sub-domains

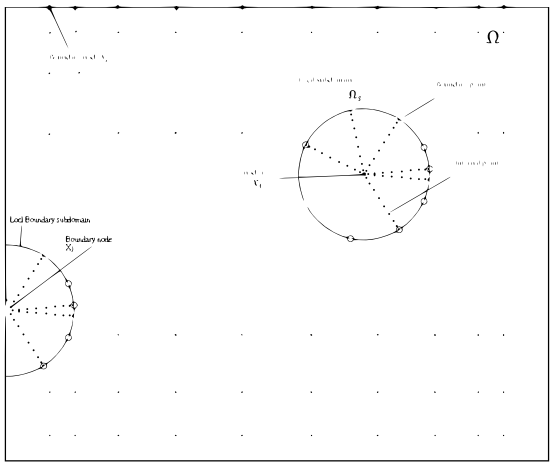

Figure 2: Distribution of integration points 10×10 in ith sub-domain Ω_s with the center at the node x_i

5 Numerical examples

Here numerical results are presented to verify the proposed method for linear PDAEs. In Examples 5.1 and 5.2 there is a comparison between the Implicit Crank–Nicolson with HCM which by Multiquadric as an RBF (ICN–HCM), the Implicit Crank-Nicolson with Multiquadric as an RBF (ICN–Kansa) in [11], the Implicit Crank-Nicolson with Quasi-Interpolation (ICN–QIE), the Implicit Crank–Nicolson with Finite Difference method (ICN–FDM) in [10] and our method.

Based on the existing different parameters in our method and their effects on the results, the same as the size of support, the number of nodes in the main domain, the radius of selected sub-domains, the number of integrating points in a sub-domain as mentioned before, in this method several parameters affects the accuracy and convergence of the problem which appear in different process of solving the problem, like writing the weak-form of the problem, partitioning the domain into sub-domains with centers determined by Gauss method, and selection of local interpolating CS-RBF instead of a trial function, also by numerically evaluating the integrals with Gauss method. For instance, determining the number of nodes in the main domain and the boundary, the size of support in the interpolating function CS–RBF trial function, selected formula, the number of integrating points in each sub-domain. By providing tables and diagrams, the more important parameters were investigated. The number of integrating points in each sub-domain, based on examining several examples were considered to be 100 points. For more information about the integrating methods, see [19] where they were discussed thoroughly.

Since using a meshfree interpolation, we numerically analyze the stability by evaluating the condition number (CN) of the interpolation matrix, which is defined by

$$CN(A) = \frac{sv_{\max}}{sv_{\min}}, \tag{5.1}$$

where $sv_{\max}$ and $sv_{\min}$ are the largest and smallest singular values of A, respectively. The result were shown in Tables 5 and 10. It is noticeable that by decreasing the separation distance $d_x = \frac{1}{2}\min_{i\neq j}||x_i - x_j||_2$, the sv_{min} approaches zero exponentially. And the growth of sv_{max} is the order of the number of the nodes. It means increasing the number of nodes to improve the accuracy could cause ill-condition matrix. So there is a contrast between accuracy and stability. As a measure of the accuracy and convergence, the absolute error, the relative error and the RMS error were evaluated. The errors are defined as

$$RMSE = \sqrt{\frac{1}{MN}\sum_{i=1}^{N}\sum_{j=1}^{M}||\Psi(x_i,t_j) - \Phi(x_i,t_j)||_2^2}, \tag{5.2}$$

$$|e_k| = |\psi_k - \phi_k|, \qquad k = 1, 2,$$

and

$$|E_k| = |\frac{\psi_k - \phi_k}{\psi_k}|, \qquad k = 1, 2, \tag{5.3}$$

where $\Phi(x,t) = \begin{pmatrix}\phi_1\\ \phi_2\end{pmatrix}$ and is the numerical solution and $\Psi(x,t) = \begin{pmatrix}\psi_1\\ \psi_2\end{pmatrix}$ is the analytical solution.

Example 5.1. Consider a linear PDAE

$$\begin{pmatrix}1 & 0\\ 0 & 0\end{pmatrix}\Psi_t + \begin{pmatrix}-1 & 0\\ 0 & -1\end{pmatrix}\Psi_{xx} + \begin{pmatrix}1 & 1\\ 1 & -4\end{pmatrix}\Psi = P(x,t),$$

where $t \in [0,1]$, $x \in [-1,1]$ and E and C are zero matrices. Also, Ψ_0, $P = \begin{pmatrix}P_1\\ P_2\end{pmatrix}$ and $\mathbf{q} = \begin{pmatrix}q_1\\ q_2\end{pmatrix}$ are chosen such that the exact solution is

$$\Psi(x,t) = \begin{pmatrix}(x^2-1)cos(\pi t)\\ x(1-x)e^{-t}\end{pmatrix},$$

and $\Phi(x,t) = \begin{pmatrix}\phi_1\\ \phi_2\end{pmatrix}$ is the numerical solution. In Tables 1 and 2, a comparison between different methods and our method with relative error (5.3) is given. In this example, different cases in terms of the number of nodes were surveyed in the Table 4. One of the most effective parameters in convergency and accuracy of the proposed method is the size of support which is surveyed for different values of s_i in Table 3.

Table 1: Comparison of the relative error between results in [10] and our method at $t = 0.3$ (Example 5.1)

	ICN-QIE		ICN-Kansa		O	ur method (ζ^6)
x	$\|E_1\|$	$\|E_2\|$	$\|E_1\|$	$\|E_2\|$	$\|E_1\|$	$\|E_2\|$
-0.95	9.10×10^{-4}	6.59×10^{-6}	6.94×10^{-2}	1.38×10^{-3}	6.74×10^{-6}	5.73×10^{-7}
-0.6	1.02×10^{-3}	8.19×10^{-5}	1.02×10^{-1}	1.57×10^{-3}	5.63×10^{-7}	1.25×10^{-6}
-0.25	1.06×10^{-3}	3.93×10^{-4}	1.05×10^{-1}	1.8×10^{-3}	4.49×10^{-7}	6.17×10^{-6}
0.1	1.07×10^{-3}	1.46×10^{-3}	1.04×10^{-1}	2.43×10^{-2}	7.18×10^{-7}	1.22×10^{-5}
0.45	8.04×10^{-3}	4.10×10^{-4}	1.01×10^{-1}	9.48×10^{-3}	4.71×10^{-7}	4.30×10^{-6}
0.8	9.64×10^{-4}	2.59×10^{-4}	8.71×10^{-2}	1.52×10^{-3}	1.03×10^{-6}	1.08×10^{-5}

Table 2: Comparison of the relative error between results in [10] and our method at $t = 0.8$ (Example 5.1)

	ICN-QIE		ICN-Kansa		O	ur method (ζ^6)
x	$\|E_1\|$	$\|E_2\|$	$\|E_1\|$	$\|E_2\|$	$\|E_1\|$	$\|E_2\|$
-0.95	1.53×10^{-3}	2.21×10^{-5}	1.37×10^{-1}	5.06×10^{-3}	1.39×10^{-7}	3.98×10^{-7}
-0.6	1.73×10^{-3}	3.19×10^{-4}	6.42×10^{-2}	7.97×10^{-3}	2.59×10^{-7}	8.29×10^{-7}
-0.25	1.83×10^{-3}	1.53×10^{-3}	6.09×10^{-2}	3.35×10^{-3}	3.41×10^{-7}	1.20×10^{-6}
0.1	1.85×10^{-3}	5.69×10^{-3}	6.01×10^{-2}	4.92×10^{-2}	3.79×10^{-8}	4.45×10^{-6}
0.45	1.78×10^{-3}	1.60×10^{-3}	6.10×10^{-2}	2.08×10^{-2}	1.70×10^{-8}	7.46×10^{-7}
0.8	1.62×10^{-3}	1.01×10^{-3}	6.95×10^{-2}	5.72×10^{-3}	6.31×10^{-7}	9.77×10^{-7}

Table 3: Comparison of the absolute error for different size of support at $t = 0.3$ and $N = 32$ (Example 5.1)

	s_i=0.5		s_i=2.5		s_i=4	
x	$\|e_1\|$	$\|e_2\|$	$\|e_1\|$	$\|e_2\|$	$\|e_1\|$	$\|e_2\|$
-0.95	2.25×10^{-2}	1.08×10^{-2}	2.66×10^{-4}	1.93×10^{-2}	2.6×10^{-4}	2×10^{-2}
-0.6	3.53×10^{-3}	6.34×10^{-3}	2.34×10^{-3}	2.54×10^{-3}	2.1×10^{-3}	2.3×10^{-3}
-0.25	2.58×10^{-3}	3.75×10^{-3}	6.66×10^{-4}	9.48×10^{-3}	7.0×10^{-4}	9.9×10^{-3}
0.1	1.73×10^{-3}	2.21×10^{-4}	1.09×10^{-3}	3.91×10^{-4}	9.8×10^{-4}	3.29×10^{-4}
0.45	3.16×10^{-3}	7.71×10^{-4}	2.85×10^{-3}	8.13×10^{-3}	2.7×10^{-3}	7.16×10^{-3}
0.8	1.01×10^{-2}	2.03×10^{-2}	3.20×10^{-4}	3.54×10^{-3}	3.25×10^{-4}	4.03×10^{-3}

Table 4: Comparison of the absolute error for different number of domain nodes at $t = 0.3$ (Example 5.1)

	N=8		N=32		N=105		N=200	
x	$\|e_1\|$	$\|e_2\|$	$\|e_1\|$	$\|e_2\|$	$\|e_1\|$	$\|e_2\|$	$\|e_1\|$	$\|e_2\|$
-0.95	2.21×10^{-1}	1.00×10^{-1}	3.80×10^{-2}	1.95×10^{-2}	4.45×10^{-2}	5.34×10^{-3}	3.86×10^{-8}	7.86×10^{-8}
-0.6	5.41×10^{-3}	6.41×10^{-3}	3.43×10^{-3}	4.09×10^{-3}	4.49×10^{-2}	3.77×10^{-2}	2.12×10^{-8}	8.89×10^{-8}
-0.25	8.53×10^{-3}	2.49×10^{-3}	4.90×10^{-3}	4.12×10^{-3}	1.92×10^{-1}	1.56×10^{-1}	2.47×10^{-8}	1.43×10^{-7}
0.1	3.20×10^{-1}	8.54×10^{-3}	5.24×10^{-3}	1.05×10^{-3}	4.88×10^{-2}	6.45×10^{-2}	4.18×10^{-8}	8.15×10^{-8}
0.45	9.92×10^{-1}	9.43×10^{-1}	4.17×10^{-3}	5.62×10^{-3}	1.10×10^{-1}	1.77×10^{-1}	2.21×10^{-8}	7.88×10^{-8}
0.8	$1.51 \times 10^{+1}$	$1.39 \times 10^{+1}$	5.88×10^{-3}	1.23×10^{-2}	1.78×10^{-3}	7.19×10^{-2}	2.19×10^{-8}	1.29×10^{-7}

Table 5: Condition number and root mean square error for different size of support and number of nodal points (Example 5.2)

	s_i=0.5		s_i=2.5		s_i=4	
N	$RMSE$	CN	$RMSE$	CN	$RMSE$	CN
8	9.41×10^{-1}	$9.58 \times 10^{+3}$	1.15×10^{-2}	$9.33 \times 10^{+3}$	2.00×10^{-2}	$1.76 \times 10^{+6}$
32	6.32×10^{-2}	$1.00 \times 10^{+15}$	1.25×10^{-3}	$4.92 \times 10^{+12}$	4.32×10^{-2}	$5.75 \times 10^{+13}$
105	3.34×10^{-2}	$2.10 \times 10^{+18}$	2.30×10^{-2}	$6.53 \times 10^{+14}$	3.53×10^{-2}	$8.72 \times 10^{+16}$
200	1.07×10^{-5}	$9.00 \times 10^{+19}$	1.12×10^{-7}	$2.05 \times 10^{+15}$	7.02×10^{-5}	$1.80 \times 10^{+18}$

Example 5.2. Consider the same problem in Example 5.1. Here, Ψ_0, $P = \begin{pmatrix} P_1 \\ P_2 \end{pmatrix}$ and $\mathbf{q} = \begin{pmatrix} q_1 \\ q_2 \end{pmatrix}$ are chosen such that

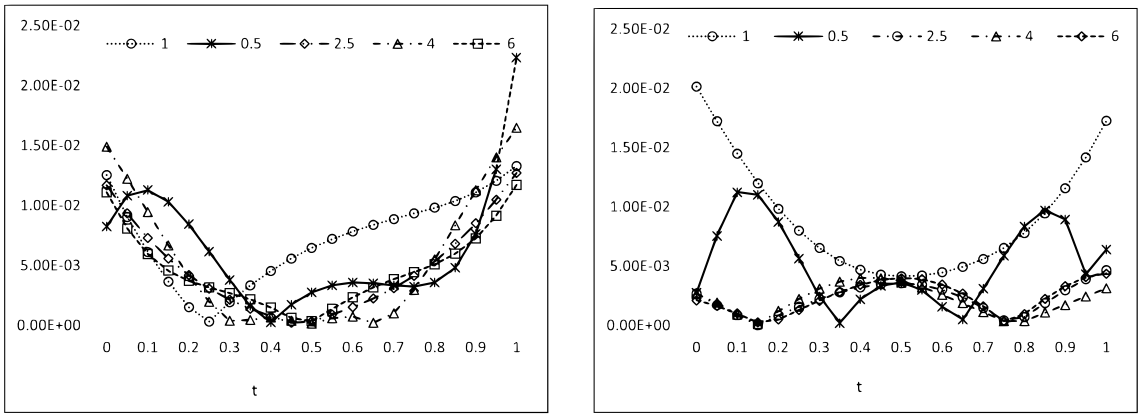

Figure 3: Comparison of the absolute error ($|E_1|$(left), $|E_2|$(right)) for different size of support for our method(ζ^6) with $N = 32$ at $x = 0.6$, (Example 5.1)

the exact solution is

$$\Psi(x,t) = \begin{pmatrix} x^5(x^2-1)cos(\pi t) \\ x^2(x^2-1)e^{-t} \end{pmatrix},$$

and $\Phi(x,t) = \begin{pmatrix} \phi_1 \\ \phi_2 \end{pmatrix}$ is the numerical solution. In this example, there are a comparison between the ICN–QIE, ICN–FDM and our method in tables 6 and 7. Also, a comparison between different cases in terms of the number of nodes in the Table 9 and different sizes of support in the Table 8 are given.

Table 6: Comparison of the relative error between results in [10] and our method at $t = 0.8$ (Example 5.2)

	ICN-QIE		ICN-FDM		O	ur method (ζ^6)
x	$\|E_1\|$	$\|E_2\|$	$\|E_1\|$	$\|E_2\|$	$\|E_1\|$	$\|E_2\|$
-0.95	1.09×10^{-4}	1.40×10^{-2}	1.53×10^{-2}	7.97×10^{0}	1.37×10^{-6}	5.46×10^{-6}
-0.6	6.05×10^{-4}	6.46×10^{-2}	6.46×10^{-2}	$2.28 \times 10^{+1}$	3.59×10^{-6}	2.12×10^{-6}
-0.25	1.58×10^{-2}	2.67×10^{0}	2.67×10^{0}	1.41×10^{0}	9.80×10^{-5}	2.51×10^{-6}
0.1	5.89×10^{-1}	$1.74 \times 10^{+2}$	$7.74 \times 10^{+2}$	$8.92 \times 10^{+2}$	1.7×10^{-2}	2.34×10^{-6}
0.45	1.70×10^{-3}	5.96×10^{-3}	5.96×10^{-3}	$4.21 \times 10^{+1}$	8.98×10^{-6}	1.94×10^{-8}
0.8	2.19×10^{-4}	1.44×10^{-2}	1.44×10^{-2}	$1.20 \times 10^{+1}$	5.26×10^{-7}	3.03×10^{-8}

Table 7: Comparison of the relative error between results in [10] and our method at $x = -0.5$ (Example5.2)

	ICN-QID		ICN-FDM		O	ur method (ζ^6)
t	$\|E_1\|$	$\|E_2\|$	$\|E_1\|$	$\|E_2\|$	$\|E_1\|$	$\|E_2\|$
0.1	1.34×10^{-4}	2.83×10^{-6}	4.70×10^{-2}	3.82×10^{0}	4.07×10^{-6}	2.26×10^{-6}
0.3	1.20×10^{-3}	1.76×10^{-5}	5.87×10^{-2}	$1.16 \times 10^{+1}$	5.58×10^{-6}	3.60×10^{-6}
0.5	$*$	3.34×10^{-5}	$*$	$1.98 \times 10^{+1}$	$*$	2.56×10^{-6}
0.7	1.88×10^{-3}	4.00×10^{-5}	1.34×10^{-1}	$2.88 \times 10^{+}$	1.79×10^{-6}	3.74×10^{-6}
0.9	7.11×10^{-4}	2.93×10^{-5}	1.30×10^{-1}	$3.89 \times 10^{+}$	3.13×10^{-6}	5.45×10^{-6}

6 Conclusion

In this paper, we considered a developed formulation of the MLPG method based on the compactly supported radial basis functions. It was successfully implemented in the numerical solution of linear partial differential equations. The proposed method was tested on examples in the form of two variables with different numbers of nodes and different sizes of support. We compared other methods with our result. The comparisons were shown in tables and figures. The results showed the validity and accuracy of the proposed method and we have got better results compared to the other methods.

Table 8: Comparison of the absolute error for different size of support at $t = 0.5$ and $N = 32$ (Example 5.2)

	s_i=0.5		s_i=2.5		s_i=4	
x	$\|e_1\|$	$\|e_2\|$	$\|e_1\|$	$\|e_2\|$	$\|e_1\|$	$\|e_2\|$
-0.95	2.4×10^{-1}	1.0×10^{-3}	3.19×10^{-3}	4.99×10^{-3}	9.90×10^{-3}	9.04×10^{-3}
-0.6	2.3×10^{-1}	9.1×10^{-3}	2.45×10^{-3}	6.07×10^{-3}	1.33×10^{-2}	6.84×10^{-3}
-0.25	6.4×10^{-2}	3.7×10^{-4}	2.93×10^{-3}	1.05×10^{-3}	1.73×10^{-2}	1.55×10^{-3}
0.1	2.7×10^{-2}	1.1×10^{-4}	2.02×10^{-3}	1.47×10^{-2}	1.12×10^{-2}	1.20×10^{-2}
0.45	5.5×10^{-2}	2.5×10^{-4}	2.89×10^{-5}	1.52×10^{-2}	1.90×10^{-3}	1.32×10^{-2}
0.8	5.8×10^{-3}	6.5×10^{-3}	1.76×10^{-3}	1.19×10^{-2}	1.24×10^{-2}	1.20×10^{-2}

Table 9: Comparison of the absolute error for different number of domain nodes at $x = 0.3$ (Example 5.2)

	N=8		N=32		N=105		N=200	
t	$\|e_1\|$	$\|e_2\|$	$\|e_1\|$	$\|e_2\|$	$\|e_1\|$	$\|e_2\|$	$\|e_1\|$	$\|e_2\|$
0.1	7.38×10^{-1}	3.24×10^{0}	5.84×10^{-2}	4.65×10^{-4}	3.52×10^{-4}	2.17×10^{-3}	6.97×10^{-8}	2.91×10^{-7}
0.3	1.09×10^{-1}	2.36×10^{0}	1.74×10^{-2}	1.22×10^{-2}	1.79×10^{-4}	2.01×10^{-3}	6.87×10^{-8}	1.95×10^{-7}
0.5	5.05×10^{-1}	1.37×10^{0}	1.32×10^{-3}	1.08×10^{-2}	3.90×10^{-5}	1.86×10^{-3}	1.20×10^{-7}	5.68×10^{-7}
0.7	8.09×10^{-1}	6.63×10^{-1}	1.65×10^{-2}	3.46×10^{-2}	8.90×10^{-5}	1.51×10^{-3}	1.01×10^{-7}	6.27×10^{-7}
0.9	8.94×10^{-1}	3.75×10^{-1}	6.12×10^{-2}	2.03×10^{-2}	2.29×10^{-4}	1.11×10^{-3}	6.39×10^{-8}	3.91×10^{-7}

Table 10: Condition number and root mean square error for different size of support and number of nodal points (Example 5.2)

	s_i=0.5		s_i=2.5		s_i=4	
N	$RMSE$	CN	$RMSE$	CN	$RMSE$	CN
8	9.65×10^{-1}	$9.58 \times 10^{+3}$	3.21×10^{-1}	$9.33 \times 10^{+3}$	1.03×10^{-1}	$1.76 \times 10^{+6}$
32	4.03×10^{-2}	$1.00 \times 10^{+15}$	1.50×10^{-2}	$4.92 \times 10^{+12}$	4.13×10^{-2}	$5.75 \times 10^{+13}$
105	7.13×10^{-3}	$2.10 \times 10^{+18}$	3.39×10^{-4}	$6.53 \times 10^{+14}$	4.71×10^{-3}	$8.72 \times 10^{+16}$
200	2.32×10^{-4}	$9.00 \times 10^{+19}$	1.27×10^{-7}	$2.05 \times 10^{+15}$	8.12×10^{-5}	$1.80 \times 10^{+18}$

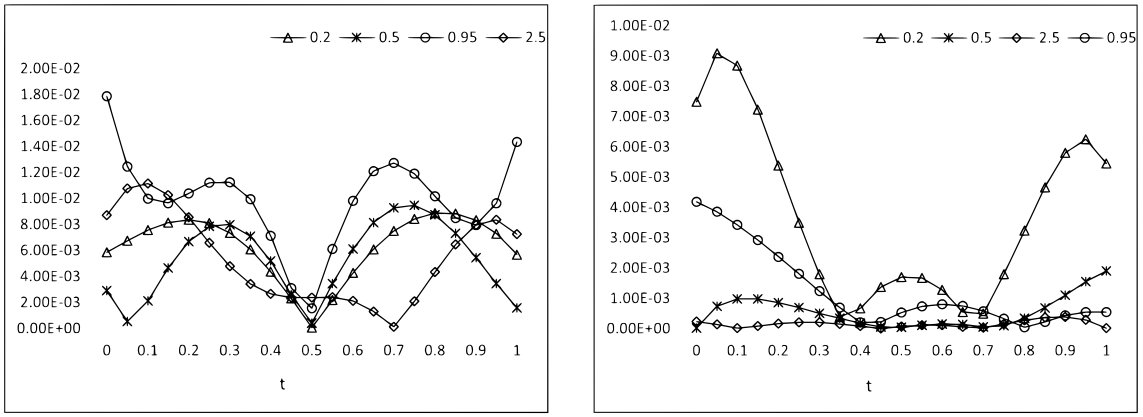

Figure 4: Comparison of the absolute error ($|E_1|$(left), $|E_2|$(right)) for different size of support for our method(ζ^6) with $N = 32$ at $x = 0.15$, Example 5.2

Acknowledgements

We are grateful to the anonymous reviewers for their helpful comments, which undoubtedly led to the definite improvement in the manuscript.

References

[1] S. Abbasbandy, H. Roohani Ghehsareh, M.S. Alhuthali and H.H. Alsulami, *Comparison of meshless local weak and strong forms based on particular solutions for a non-classical 2-D diffusion model*, Eng. Anal. Bound. Elem.

39 (2014), 121–128.

[2] S. Abbasbandy and A. Shirzadi, *A meshless method for two–dimensional diffusion equation with an integral condition*, Eng. Anal. Bound. Elem. **34** (2010), 1031–1037.

[3] H. Almasieh and J. Nazari Meleh, *Hybrid functions method based on radial basis functions for solving nonlinear fredholm integral equations*, J. Math. Exten. **17** (2013), no. 3, 29–38.

[4] S.N. Atluri, *Methods of Computer Modeling in Engineering and Sciences*, Tech. Science Press, 2002.

[5] S.N. Atluri, H.G. Kim and J.Y. Cho, *A critical assessment of the truly meshless local Petrov–Galerkin (MLPG) and local boundary integral equation (LBIE) methods*, Comput. Mech. **24** (1999), 348–372.

[6] S.N. Atluri and S. Shen, *The meshless local Petrov-Galerkin (MLPG) method: A simple and less-costly alternative to the finite element and boundary element methods*, Comput. Model. Engrg. Sci. **3** (2002), no. 1, 11–52.

[7] S.N. Atluri and T. Zhu, *A new meshless local Petrov-Galerkin (MLPG) approach in computational mechanics*, Comput. Mech. **22** (1998b), 117–127.

[8] S.N. Atluri and T. Zhu, *A new meshless local Petrov-Galerkin (MLPG) approach to nonlinear problems in computational modeling and simulation*, Comput. Model. Simul. Engrg. **3** (1998a), 187–196.

[9] S.N. Atluri and T. Zhu, *New concepts in meshless methods*, Int. J. Numer. Mech. Engrg. **47** (2000), 537–556.

[10] W. Bao and Y. Song, *Multiquadric quasi-interpolation methods for solving partial differential algebraic equations*, Numer. Meth. Partial. Differ. Eq. **30** (2014), 95–119.

[11] W. Bao and Y. Song, *Solving partial differential algebraic equations by collocation and radial basis functions*, J. Appl. Math. Inf. **30** (2012), no. 5-6, 951–969.

[12] Y. Duan, P.F. Tang and T.Z. Huang, *A novel domain decomposition method for highly oscillating partial differential equations*, Eng. Anal. Bound. Elem. 33 (2009), no. 11, 1284–1288.

[13] P. González-Casanova, J. A. Mũnoz-Gómez and G. Rodríguez-Gómez, *Node adaptive domain decomposition method by radial basis functions*, Numer. Meth. Partial. Diff. Eq. **25** (2009), no. 6, 1482–1501.

[14] M. Hajiketabi and S. Abbasbandy, *The combination of meshless method based on radial basis functions with a geometric numerical integration method for solving partial differential equations: Application to the heat equation*, Eng. Anal. Bound. Elem. **87** (2018), 36–46.

[15] K. Li, Q.B. Huang, J.L. Wang and L.G. Lin, *An improved localized radial basis function meshless method for computational aeroacoustics*, Eng. Anal. Bound. Elem. **35** (2011), no. 1, 47–55.

[16] L. Ling and E.J. Kansa, *A least-squares preconditioner for radial basis functions collocation methods*, Adv. Comput. Math. **23** (2005), no. 1-2, 31–54.

[17] G.R. Liu and Y.T. Gu, *A local radial point interpolation method (LRPIM) for free vibration analysis of 2-D solids*, J. Sound Vib. **246** (2001), 29–46.

[18] W. Marszalek, *Analysis of Partial Differential Algebraic Equations*, PhD Thesis, North Carolina Stat University, Raleigh, NC, USA, 1997.

[19] A. Mazzia and G. Pini, *Product Gauss quadrature rules vs.cubature rules in the meshless local Petrov-Galerkin method*, J. Complexity **26** (2010), 82–101.

[20] R. Schaback, *Error estimates and condition numbers for radial basis function interpolation*, Adv. Comput. Math. **3** (1995), no. 3, 251–264.

[21] F. Soltanian, M. Dehghan and S.M. Karbasi, *Solution of the differential algebraic equations via homotopy perturbation method and their engineering applications*, Int. J. Comput. Math. **87** (2010), no. 9, 1950–1974.

[22] H. Wendland, *Piecewise polynomial, positive definite and compactly supported radial basis functions of minimal degree*, Adv. Comput. Math. **4** (1995) 389–396.

[23] H. Wendland, *Error estimate for interpolation by compactly supported radial basis function of minimal degree*, J. Approx. Theory **93** (1998), 258–272.

[24] Z. Wu and R. Schaback, *Local error estimate for radial basis function interpolation of scattered data*, IMA J. Numer. Anal. **13** (1993), 13–27.

[25] Z. Wu, *Compactly supported positive definite radial functions*, Adv. Comput. Math. **4** (1995), 283–292.

[26] J.R. Xiao and M.A. McCarthy, *A local Heaviside weighted meshless method for two-dimensional solids using radial basis functions*, Comput. Mech. **31** (2003), 301–315.

[27] F. Zhou, J. Zhang, X. Sheng and G. Li, *Shape variable radial basis function and its application in dual reciprocity boundary face method*, Eng. Anal. Bound. Elem. **35** (2011), no. 2, 244–252.